A comparative study of Graphite and Silicon as suitable substrates for the self-catalyzed growth of InAs nanowires by MBE

Anyebe, Ezekiel A[1, †,*], Kesaria, Manoj[2], Sanchez, A. M[3]., Qiandong Zhuang[1]

[1]Physics Department, Lancaster University, Lancaster LA1 4YB, UK

[2]School of Physics and Astronomy, Cardiff University, Cardiff, UK

[3]Department of Physics, Warwick University, Coventry CV4 7AL, U.K.

*E-mail- ezeanyabe@hotmail.co.uk

Abstract

In order to fully exploit the enormous potential of functional monolithic nanowire/graphene hybrid structures in high performance flexible devices, a better understanding of the influence of the graphitic substrate (GS) on NWs growth is crucial. InAs nanowires (NWs) were simultaniously grown on Si and GS with identical growth temperature, In-flux and V/III flux ratio via an In-catalyzed growth technique. It is demonstrated that the GS is a more favourable platform for the growth of dense InAs NWs under highly In-rich conditions (low V/III flux ratio), whereas Silicon is a more suitable substrate under a highly As-rich condition (high V/III flux ratio). It is shown that the GS enables NWs growth at high In-flux which has enormous potential for the fabrication of cost-effective nanodevices. Transmission electron microscopy analysis of the NW/GS interface confirms the NWs are well aligned on the graphitic substrate. This study opens new possibilities for the choice of suitable substrate for the optimal growth of NWs under various conditions.

Keywords: self-catalyzed, InAs, Nanowires, Graphite, density

[†]Present address: Federal University of Agriculture, Makurdi, PMB 2373, Nigeria

1. Introduction

Over the last few years the advent[1,2] of graphene, the two dimensional (2D) single layer carbon material, has sparked enormous research interest owing to its extraordinary electronic and optical properties including ultra-high carrier mobility[3,4], exceptionally high thermal conductivity, flexibility and high optical transparency[5,6] which offers huge promise for applications in transparent and stretchable electronics. It's relative abundance and scalability further provides greater opportunities for large scale fabrication[7–9]. Its high electron mobility, high elastic modulus and versatility has made it ideal for use as a substrate[10–12].

Graphene–NWs hybrid structures have drawn enormous attention in order to exploit the exceptional qualities of the graphitic substrate as well as the intriguing properties of NWs including epitaxial growth insensitive to lattice mismatch[13] for applications in high performance, flexible and cost-effective functional devices. InAs NWs are particularly interesting for applications in high-speed electronics and mid-infrared devices [14,15] due to their narrow direct bandgap, small electron effective mass and high electron mobility[16,17]. In such hybrid architectures, the two dimensional graphene substrate can function as an ideal electrode because of its high transparency, high conductance and excellent chemical stability[18,19]. Several graphene-based devices including transistors[20–23], light emitting diodes[24,25], supercapacitors[26], photodetectors[27], gas detectors[28], photovoltaic electrodes[29] and devices[10,30–32], flexible antennas[33] and foldable energy-storage devices[34] have been demonstrated. However, despite significant advances, the development of flexible devices based on van der Waals heterostructures is not without some challenges including the poor on/off current switching of graphene resulting from its zero-band gap. Interestingly, recent studies[35] indicates that graphene has the ability to exhibit semiconducting properties, which could potentially allow for its use in the next generation of future high-performance, ultrafast, flexible electronic devices.

Graphene/graphitic substrates (GS) have been touted as a potential replacement to current silicon-based electronics which is approaching the limit of improvements to performance and capacity through dimensional scaling[36,37]. In order to integrate semiconductor NWs with the GS, a better understanding of the influence of the GS on NWs growth is crucial for the development of high performance flexible nanodevices. Compared to the conventional growth of InAs NWs on rigid Si substrates which is well-established[13,17,38–40], the noncovalent van der waals epitaxy (VDWE) growth of InAs NWs on 2D GS is still in its early stages and requires increased research activity to fully exploit its enormous potential for functional monolithic NWs/graphene hybrid structures. In a previous study[41], we demonstrated that the graphitic substrate is a favourable platform for the growth of high quality, vertically aligned, non-tapered and ultrahigh aspect ratio $InAs_{1-x}Sb_x$ NWs. Given the significant differences in the mechanism of epitaxial growth, it is essential to investigate whether the morphology and density of InAs NWs grown via conventional heteroepitaxy on Si could be achieved by the non-covalent VDWE on the GS. Recently, it has been demonstrated that the THz emission efficiency[42] as well as the photocurrent and power conversion of solar cells[43] can be significantly improved by increasing the NWs length (aspect ratio). Consequently, it is paramount to investigate the effect of the GS on the yield, morphology and axial growth rate of NWs which are very crucial for high performance nanodevices[42–46].

In this work, the growth of InAs NWs on GS is systematically investigated in comparison to that on Si with a view to better understanding the influence of the substrates on NWs growth. It is demonstrated that the GS is a more favourable platform for the growth of dense InAs NWs under In-rich conditions (low V/III flux ratio) whereas the Si substrate is a more suitable substrate for realizing a high yield of InAs NWs under highly As-rich conditions (high V/III flux ratio).

2. Experimental details

InAs NWs growth was performed on GS by solid-source molecular beam epitaxy (MBE) via an indium droplet-assisted growth technique. Mechanically exfoliated graphite films from highly oriented pyrolytic graphite (HOPG) were transferred onto Si (111) substrates and thermally outgassed in the system. In order to investigate the substrate effect on the yield and morphology of InAs NWs, the GS and bare Si were Indium bonded onto the same sample holder and loaded into the MBE system for outgassing and subsequently transferred into the growth chamber for InAs NWs growth. The substrate temperature was measured with a thermocouple and there was no significant variation in temperature in different portions of the substrate. The Si substrates were chemically cleaned by dipping in 12% hydrofluoric acid solution for ~3 minutes to remove the native oxide and quickly loaded into the MBE system to avoid re-oxidation. In droplets were then deposited[39] and the growths performed simultaneously on both GS and silicon substrates under identical growth conditions. InAs NWs growth commenced with the opening of In and As shutters concurrently to allow for the introduction of growth species. As_4 was utilized for the NWs growth. In order to gain detailed insight into the influence of the GS under various growth conditions, the highly essential growth parameters of temperature, In-flux and V/III flux ratio were independently varied. High-resolution transmission electron microscope (HRTEM) images were taken in a JEOL-JEM 2100 working at 200 kV. Focused ion beam (FIB) specimens were prepared using a JIB4500 to investigate the interface with the substrate.

Three sets of samples were grown independently by tuning the growth temperature (T_G), In-fluxes and V/III flux ratio ($F_{V/III}$). The first set of samples were grown for ~ 60 minutes at a fixed In-flux of 1.8 x 10^{-7} mbar and $F_{V/III}$ of 55 while T_G was varied from 400 to 475^{o}C to investigate the influence of the GS on NWs growth as a function of temperature. A second set

of samples were grown at a constant $F_{V/III}$ and T_G of 55 and 450 ºC respectively while varying In-fluxes in the range of (1.8 - 2.4) x 10^{-7}mbar for ~ 60 minutes. The last set of samples were then grown at various $F_{V/III}$ ranging from 27 to 55 at a fixed T_G of 450 ºC and In-flux of 10^{-7} mbar for 20 minutes. FEI XL30 SFEG scanning electron microscope (SEM) was used for determining the surface morphology of as grown NWs. FEI XL30 SFEG scanning electron microscope (SEM) was used for determining the surface morphology of as grown NWs.

3. Influence of the Graphitic Substrate on Nanowire Growth

Figure 1 shows the scanning electron microscope (SEM) images of InAs NWs grown on GS as a function of temperatures (T_G), the SEM images of NWs grown simultaneously on Si is also shown. Although both GS and Si substrates display a high density of islands (clusters) at a low temperature of 400ºC, a relatively high yield of NWs (6.47 ×10^7 cm^{-2}) was obtained on GS when compared to Si (3.66 ×10^7 cm^{-2}). Note that the NWs yield was mostly estimated from ~70% of measurable NWs manually counted from at least two SEM images taken from different sections of each sample to compensate for any slight variation in temperature on the sample surface. Tilted view SEM images were used for measurement of the length of as-grown InAs NW with ~70% of measurable NWs in each sample utilized. Gaussian approximations were then used for the determination of the error bars of the NWs geometry which is expressed as the deviation from the mean geometry of normally distributed NWs. Nanostructures with diameters constrained to 1 – 100 nm are termed NWs whereas those with diameters exceeding 100nm are regarded as nanorods. However, given the obvious limitations of SEM, structures with sizes slightly exceeding this range are still viewed as NWs. Most of the nanostructures obtained in this work have their diameter within the NWs range and were thus used for the determination of NWs yield.

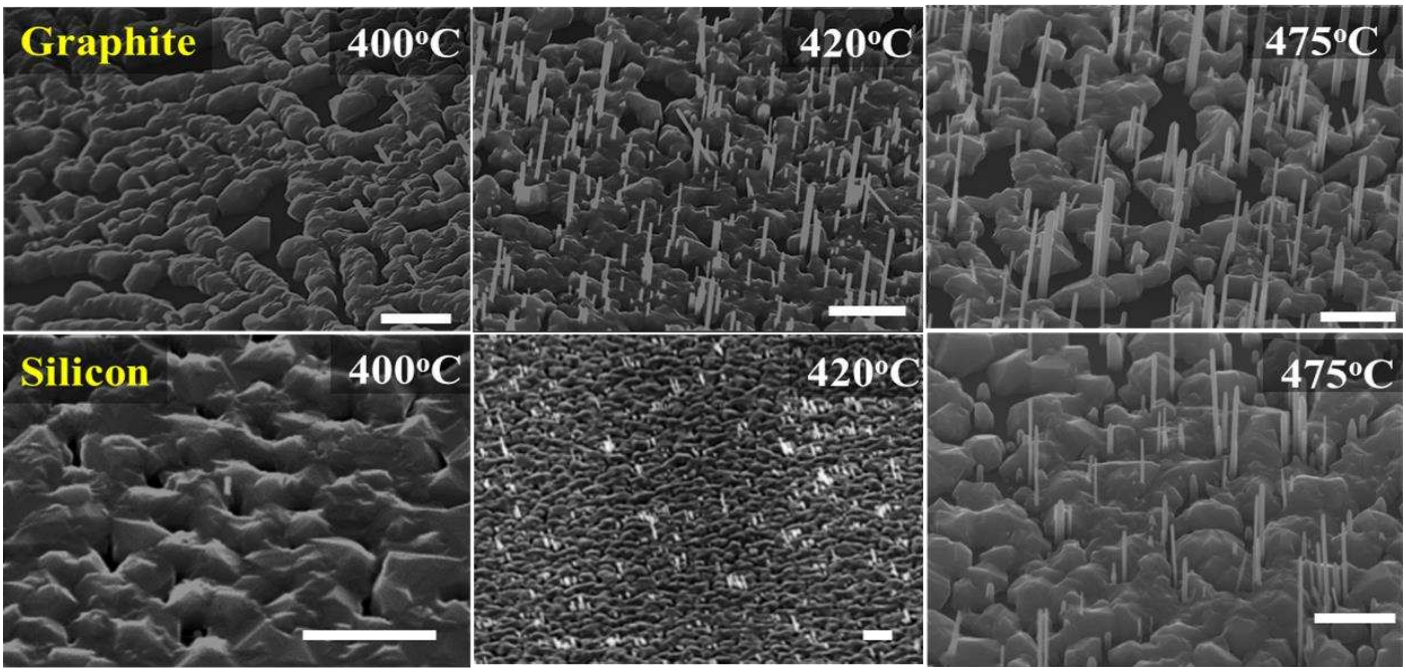

Figure 1: Tilted SEM images of InAs NWs grown on graphitic and Si substrates as a function of growth temperature.

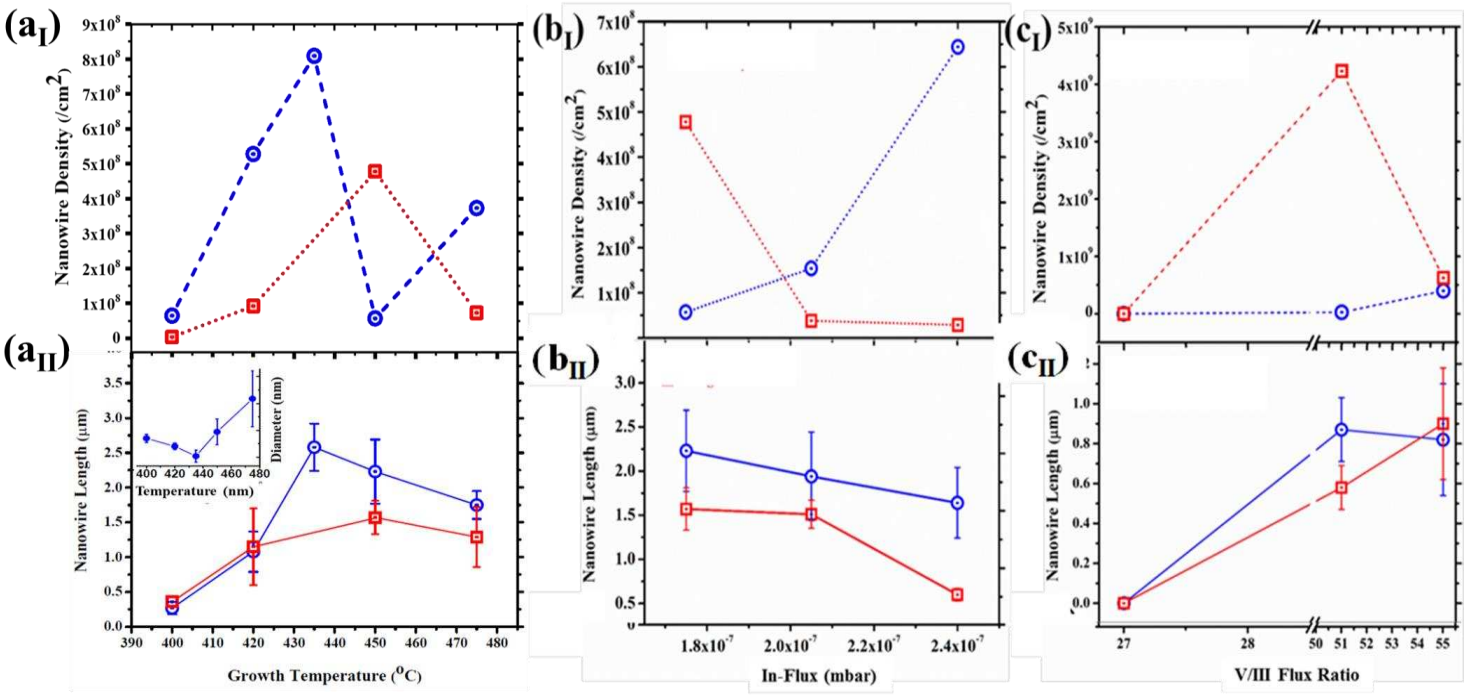

Figure 2: Comparison of the influence of growth temperature (a_{I-II}); In-Flux (b_{I-II}) and V/III flux ratio (c_{I-II}) on InAs nanowires density (top panel) and length (bottom panel) grown on graphitic (⊙) and silicon (⊡) substrates. The inset of Figure a_{II} shows the plot of Nanowire diameter versus growth temperature.

A slight increase in growth temperature to 420°C was accompanied by a significant increase in NWs yield on the GS to about ~6 times that on Si. As can be clearly seen in Figure 2a$_I$, a similar trend was also observed for a further increase in T_G with the NWs on GS displaying a significantly higher yield of vertically-aligned NWs. This demonstrates that the GS is more favourable for realizing a high yield of InAs NWs than Si which could be attributed to the nearly coherent lattice matching between InAs <110> and graphene <1000> resulting in a relatively small lattice mismatch of ~ 0.5%[47–49] compared to the high mismatch of the InAs-Si system (~11.6 %)[50,51]. In addition, the absence of dangling bonds on the GS minimizes the influence of strain and promotes the growth of a highly dense array of NWs.

As can be observed, the InAs NWs density on both substrates initially increased and then decreased with increasing temperature. This is attributed to the temperature dependence of adatom diffusion. At a relatively low temperature, adatom diffusion is limited leading to the growth of a high density of small Indium droplets which do not meet the critical diameter criterion for nucleating NWs due to their limited size[39] which is ascribed to the Gibbs–Thomson effect[52,53] which defines the thermodynamic dependence of the chemical potential and NWs growth rate on the curvature and hence the diameter of the nucleating droplet. However, at moderately high temperatures, adatom diffusion length is increased and a high density of optimal droplets[39] are realized promoting a high density of NWs. Finally, for a further increase in temperatures, extremely large nucleation droplets merge to form clusters and are consumed at the early stages of NW growth resulting in a decline in NWs density. More so, the desorption rate of the droplets is significantly increased at high temperatures leading to fewer NWs nucleation[54]. To elucidate the influence of the substrates on NWs morphology, the geometry of InAs NWs grown on both substrates was evaluated. Figure 2a$_{II}$ shows the dependence of NWs lengths (L_{NW}) on T_G. The error bars of

L_{NW} which is the deviation from the mean geometry of normally distributed NWs were obtained from over 70% of measurable NWs. It clearly shows the NWs on GS are relatively longer than the ones on Si. A maximum L_{NW} of ~3 µm was achieved on GS while only ~2 µm long NWs was obtained on Si for the investigated temperature range (400-475°C). As shown in the inset of Figure 2a_{II}, the diameter of the NWs scales inversely with L_{NW} for $G_T \leq 435$°C followed by the reverse effect for a further rise in temperature on the GS which is indicative of a diffusion limited growth. The slightly higher NWs length on GS in comparison to Si can be attributed to the high thermal conductivity of HOPG which is among the highest of any known material, about 2000 W m^{-1} K^{-1} (in-plane)[55,56] and even higher values of 2000–4000 W m^{-1} K^{-1} at room temperature for freely suspended Graphene[57–60]. In comparison, the thermal conductivity of Silicon is only about 149 W m^{-1} K^{-1}[61,62]. This implies the effective growth temperature of the NWs on the GS is relatively higher than that on Si (although, both substrates were placed in the same MBE chamber and simultaneously set at the same temperature at growth initiation), consequently, adatom kinetic energy and mobility is enhanced on the graphitic substrate. NWs with an ultrahigh aspect ratio of over ~80 was realized on GS whereas an aspect ratio of only ~25 was obtained on Silicon.

Considering the influence of In-flux, we observed NWs growth was limited on both substrates (not shown) at a relatively low In flux (1.8 x 10^{-7} mbar). However a slight increase in In-flux to 2.1 x 10^{-7} mbar was accompanied by about 3-fold increase in NWs density on GS while there was nearly 12-fold decrease in NWs yield on Si (Figure 3). Importantly, when the In-flux was slightly raised to 2.4 x 10^{-7}mbar, the NWs yield was over 20x higher on GS in comparison to

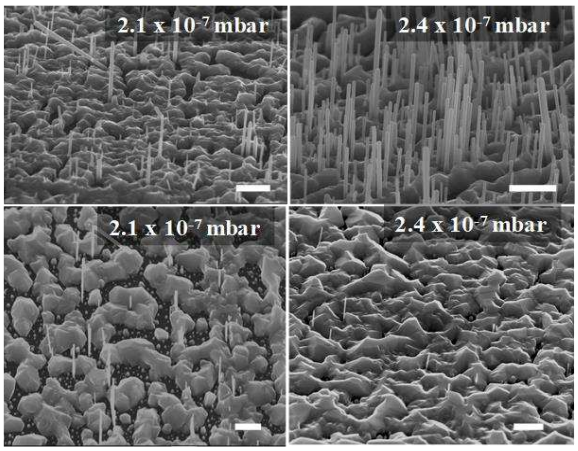

Figure 3: InAs nanowires grown on graphitic (top panel) and Silicon (Bottom panel) substrates at a constant temperature and As-fluxes but varying In-fluxes. The Scale bars correspond to 1 µm.

Si (Figure 2b$_I$). Conversely, there was a predominant growth of Islands on the Si substrate at the same In-flux. This could be attributed to the fact that a high In-flux results in the deposition of a high density of small droplets resulting from the reduced adatom diffusion time[39]. Owing to the fact that only moderately large droplets (with diameter ≥70 nm) contribute to the nucleation of InAs NWs[39], it is understandable that a high In-Flux results in increased growth of Islands almost coalesced into a film on Si (Figure 3) with a corresponding decline in NWs yield. Conversely, the enhancement in NWs yield on GS as a function of In-Flux can be correlated with an increase in NWs nucleation probability resulting from the high density of suitably large optimal nucleation droplets (thanks to the relatively high temperature of the graphitic substrate associated with its high thermal conductivity). This demonstrates that compared to conventional Si, the GS is a more favourable platform for the self catalyzed growth of densely packed and vertically-aligned, high aspect ratio NWs under highly In-rich conditions (low V/III flux ratio). This also demomnstrates that the graphitic substrate is highly promising for the fabrication of cost-effective nanodevices since it enables NWs growth at high In-flux. Considering the influence of In-flux on NWs geometry, it can be seen from Figure 2b$_{II}$ that the NWs on GS are longer than the ones on Si for the investigated range of In flux [(1.8 - 2.4) x 10^{-7}mbar]. For instance, at an In-flux of 2.4 x 10^{-7}mbar, the NWs length on GS is almost 3× that on Si (~0.60µm) which further demonstrates that axial NWs growth is promoted by the GS.

Turning to the influence of the GS under various V/III flux ratio ($F_{V/III}$), although the evolution from the islands morphology to NWs structures was realized on both substrates at a relatively high $F_{V/III}$ of 51, NWs nucleation on Si is more strongly influenced by the $F_{V/III}$ (Figure 4). Specifically, at a $F_{V/III}$ of 51, the density (4.23 x 10^9 cm^{-2}) of vertically aligned NWs on Si was about an order of magnitude higher than those on the GS as depicted in Fig. $2c_I$ (upper panel). A further increase in As-flux ($F_{V/III}$ = 55) yielded a dense array (~ 6.25 x 10^8 cm^{-2}) of NWs on Si, whereas a sparse distribution of NWs (~2.55 x 10^7 cm^{-2}) was obtained on GS (Fig. $2c_I$). The low NWs yield on GS could be associated with the insufficient supply of the volatile As specie which has a relatively high vapour pressure (15 Torr)[63] due to its evaporation from the thermally reactive GS substrate. The statistically significant difference in yield elucidates the substrate effect on InAs NWs growth. This demonstrates that compared to the GS, Si is a more favourable substrate for the growth of a dense array of NWs under highly As-rich conditions (high V/III flux ratio). However, axial NWs growth on both substrates is enhanced by As-rich conditions (Figure $2c_{II}$) with no significant influence of the substrates on NWs length.

To further investigate the growth of InAs NWs on Si and graphite substrate under different growth condition, we adapt the "As-only" model[64] which is based on the assumption that surface diffusion of As species provides at most a minor contribution to NWs growth. It presumes NWs growth rate is As-concentration dependent with the diameters of NWs almost fixed during growth confirmed by little or no change the droplet volume (and hence number of In atoms contained therein). It posits that during NWs growth As atoms are added to the droplet via two major pathways (i) direct impingement of As molecules on the droplet from the As source and (ii) by re-emission of As from the nearby neighboring surfaces of the substrate. Conversely, As is consumed by (i) the nucleating NW at the solid-liquid interface for axial NW growth (ii) evaporation from the droplet. The measured axial NWs growth rate (τ_m) (which in

effect determines L_{NW}) is the algebraic sum of contributions from the direct As flux (τ_d), re-emitted As species by the surfaces of the substrate and the neighboring NWs (τ_r), as well as the evaporated atomic flux (τ_e) as shown below:

$$\tau_m = \tau_d + \tau_r - \tau_e \quad (1)$$

τ_d depends exclusively on the direct As flux and unchanged for the NWs on both Si and graphite substrates since they were grown simulataniously with the same experimental conditions. On the other hand, the re-emitted (τ_r) contribution which is dependent on the NWs distribution (NWs neighbourhood) and the substrate and is given by [61]:

$$\tau_r = \xi\tau_d \quad (2)$$

Where ξ is a NW-specific coefficient which depends on the In droplet contact angle β and NWs distribution. Although, ξ is not expected to vary for monosubstrate NW growth, given the differences in chemical bonding and spartial NWs distribution, there is the possibility that ξ contributes to the observed variation in NWs geometry on both substrates. Furthermore, since τ_r is also dependent on the nature of the substrate (in addition to the neighboring NWs), we introduce a substrate dependent parameter Ψ, such that:

$$\tau_r = \Psi\xi\tau_d \quad (3)$$

Ψ depends on substrate specific parameters including thermal conductivity which is significantly different between Si and the GS (as previously discussed above). It is believed that the high thermal conductivity of the GS in comparison to Si would promote τ_e in favour of τ_r .The significantly high As-re-emission on GS would naturally enhance NW nucleation at

the solid-liquid interface promoting high axial growth. This further explains why the NWs on graphite are longer than their counterparts on Si under different growth conditions (Figure 2). Specifically, the influence of contributions from As- re-emission is expected to be more significant at higher growth temperatures. This could further explain the significant variation in NWs axial growth with increasing temperature beyond 420^0C evidenced by longer NWs on the GS in comparison to Si. This is in addition to the increased adatom diffusion on the GS as earlier explained. The effect of re-emitted As contributions when the In-fluxes (constant temperature and V/III flux ratio) was varied is expected to be more significant since more As-species are made available to facilitate NWs growth. It is therefore not surprising that longer L_{NW} was obtained on graphite than Si for all range of In-fluxes employed for this study. Similarly, the longer NWs observed on the GS when the V/III flux ratio was varied could partly be associated to the contributions from the re-emitted As species due to increased nucleation rate with high As flux. As regards the evaporated atomic flux (τ_e), it is believed that the evaporation current of a given atom or molecule is proportional to its equilibrium pressure with the liquid. Similarly, in the bulk liquid phase, the equilibrium pressure depends exclusively on temperature and As atomic concentration [65]. The As specie is the most likely candidate to evaporate from the droplet (as against In) during NWs growth due to its high vapour pressure [62]. However, we do not anticipate any significant difference in evaporated atomic As flux from the droplet on both substrates.

In order to gain insight into the structure of the InAs NWs/GS interface, Transmission electron microscopy (TEM) experiments were conducted and compared to that of Si. Similar to the InAs NW on Si (Fig. 5a), the InAs NWs are vertically well-aligned on the GS (InAs[111]‖-graphite[0001]) as shown in Figs. 5b-c. The fast Fourier transform (FFT) image in (Fig. 5d) further confirms that the NWs are aligned to the GS.

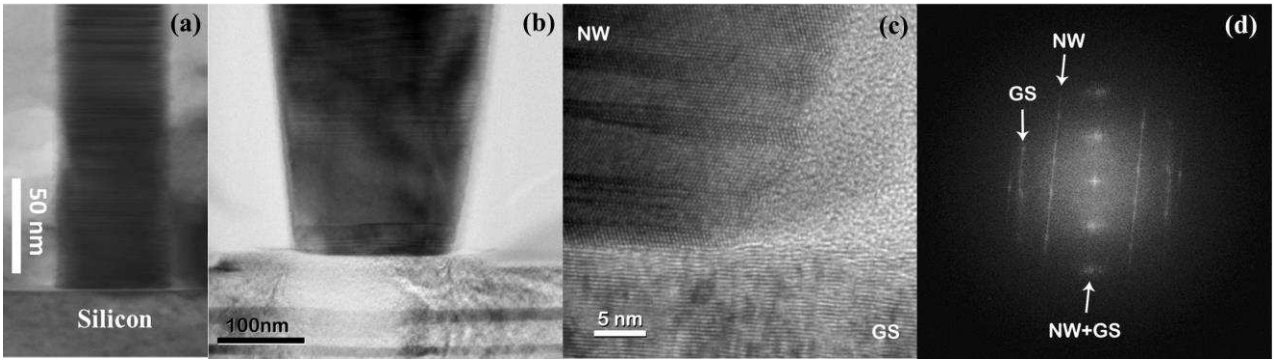

Figure 5: TEM images of InAs NW on Silicon (a) and GS (b). High resolution TEM image (c) and Fast Fourier transform (FFT) image (d) at the interface between NW and the GS.

5. Conclusions

In summary, it is demonstrated that the GS is a more favourable substrate for the growth of InAs NWs under highly In-rich conditions (low V/III flux ratio) whreas Si is preferable under highly As-rich conditions (high V/III flux ratio). Transmission electron microscopy analysis reveals the InAs NWs are vertically well-aligned on the GS.

Conflicts of interest

There are no conflicts of interest to declare

Acknowledgments

The authors are thankful for the financial support received from EPSRC Lancaster IAA, Gas Sensing Solutions Ltd, UK and Tertiary Education Trust Fund (TETFund), Nigeria.

References

1 K. S. Novoselov, D. Jiang, F. Schedin, T. J. Booth, V. V Khotkevich, S. V Morozov and A. K. Geim, *Proc. Natl. Acad. Sci. U. S. A.*, 2005, **102**, 10451–10453.

2 K. S. Novoselov, A. K. Geim, S. V Morozov, D. Jiang, Y. Zhang, S. V Dubonos, I. V Grigorieva and A. A. Firsov., *Science (80-.).*, 2004, **306**, 666–669.

3 K. S. Novoselov, A. K. Geim, S. V. Morozov, D. Jiang, M. I. Katsnelson, I. V. Grigorieva, S. V. Dubonos and A. A. Firsov, *Nature*, 2005, **438**, 197–200.

4 Y. Zhang, Y.-W. Tan, H. L. Stormer and P. Kim, *Nature*, 2005, **438**, 201–204.

5 A. K. Geim and K. S. Novoselov, *Nat. Mater.*, 2007, **6**, 183–191.

6 Z.-S. Wu, W. Ren, L. Gao, J. Zhao, Z. Chen, B. Liu, D. Tang, B. Yu, C. Jiang and H.-M. Cheng, *ACS Nano*, 2009, **3**, 411–417.

7 L. G. De-Arco, Y. Zhang, C. W. Schlenker, K. Ryu, M. E. Thompson and C. Zhou., *Nano. Lett.*, 2010, **4**, 2865–2873.

8 X. Li, W. Cai, J. An, S. Kim, J. Nah, D. Yang, R. Piner, A. Velamakanni, I. Jung, E. Tutuc, S. K. Banerjee, L. Colombo and R. S. Ruoff., *Science (80-.).*, 2009, **324**, 1312–1314.

9 J. P. Alper, A. Gutes, C. Carraro and R. Maboudian, *Nanoscale*, 2013, **5**, 4114–4118.

10 P. K. Mohseni, A. Behnam, J. D. Wood, X. Zhao, K. J. Yu, N. C. Wang, A. Rockett, J. A. Rogers, J. W. Lyding, E. Pop and X. Li., *Adv. Mater.*, 2014, **26**, 3755–3760.

11 K. Chung, H. Yoo, J. K. Hyun, H. Oh, Y. Tchoe, K. Lee, H. Baek, M. Kim and G.-C. Yi, *Adv. Mater.*, 2016, **28**, 7688–7694.

12 J. E. Choi, J. Yoo, D. Lee, Y. J. Hong and T. Fukui, *Appl. Phys. Lett.*, 2018, **112**, 142101.

13 W. Wei, X. Y. Bao, C. Soci, Y. Ding, Z. L. Wang and D. Wang, *Nano Lett.*, 2009, **9**, 2926–2934.

14 N. Guo, W. Hu, L. Liao, S. Yip, J. C. Ho, J. Miao and Z. Zhang, *Adv. Mater.*, 2014, **26**, 8208–8209.

15 F. Hehai, H. Weida, P. Wang, N. Guo, W. W. Luo, D. Zheng, F. Gong, M. Luo, H. Tian, X. Zhang, C. Luo, X. Wu, P. Chen, L. Liao, A. Pan and X. Chen, *Nano Lett.*, 2016, **16**, 6416–6424.

16 X. Wallart, J. Lastennet, D. Vignaud and F. Mollot, *Appl. Phys. Lett.*, 2005, **87**, 43504.

17 S.-G. Ihn and J.-I. Song., *Nanotechnology*, 2007, **18**, 355603.

18 X. Huang, Z. Zeng, Z. Fan, J. Liu and H. Zhang, *Adv. Mater.*, 2012, **24**, 5979–6004.

19 H. Kim, S. H. Bae, T. H. Han, K. G. Lim, J. H. Ahn and T. W. Lee, *Nanotechnology*, 2014, **25**, 14012.

20 L. Liao, Y. C. Lin, M. Q. Bao, R. Cheng, J. W. Bai, Y. A. Liu, Y. Q. Qu, K. L. Wang, Y. Huang and X. F. Duan, *Nature*, 2010, **467**, 305–308.

21 J. O. Hwang, D. H. Lee, J. Y. Kim, T. H. Han, B. H. Kim, M. Park, K. No and S. O. Kim, *J. Mater. Chem.*, 2011, **21**, 3432–3437.

22 L. Britnell, R. V Gorbachev, R. Jalil, B. D. Belle, F. Schedin, A. Mishchenko, T. Georgiou, M.

I. Katsnelson, L. Eaves, S. V Morozov, N. M. R. Peres, J. Leist, A. K. Geim, K. S. Novoselov and L. A. Ponomarenko, *Science (80-.).*, 2012, **335**, 947–950.

23 T. Georgiou, R. Jalil, B. D. Belle, L. Britnell, R. V Gorbachev, S. V Morozov, Y.-J. Kim, A. Gholinia, S. J. Haigh, O. Makarovsky, L. Eaves, L. A. Ponomarenko, A. K. Geim, K. S. Novoselov and A. Mishchenko, *Nat. Nanotechnol.*, 2013, **8**, 100–103.

24 M. Tchernycheva, P. Layenus, H. Zhang, A. V Babichev, G. Jacopin, M. Shahmohammadi, F. H. Julien, R. Ciechonski, G. Vescovi and O. Kryliouk, *Nano Lett.*, 2014, **14**, 2456–2465.

25 F. Withers, O. Del Pozo-Zamudio, A. Mishchenko, A. P. Rooney, A. Gholinia, K. Watanabe, T. Taniguchi, S. J. Haigh, A. K. Geim, A. I. Tartakovskii and K. S. Novoselov, *Nat. Mater.*, 2015, **14**, 301–306.

26 S. D. Perera, M. Rudolph, R. G. Mariano, N. Nijem, J. P. Ferraris, Y. J. Chabal and K. J. Balkus, *Nano Energy*, 2013, **2**, 966–975.

27 J. Miao, W. Hu, N. Guo, Z. Lu, X. Liu, L. Liao, P. Chen, T. Jiang, S. Wu, J. C. Ho, L. Wang, X. Chen and W. Lu, *Small*, 2015, **11**, 936–942.

28 V. V Quang, N. V Dung, N. S. Trong, N. D. Hoa, N. V Duy and N. V Hieu, *Appl. Phys. Lett.*, 2014, **105**, 13107.

29 C.-D. Kim, N. T. N. Truong, V. T. H. Pham, Y. Jo, H.-R. Lee and C. Park, *Mater. Chem. Phys.*, 2019, **223**, 557–563.

30 L. Britnell, R. M. Ribeiro, A. Eckmann, R. Jalil, B. D. Belle, A. Mishchenko, Y. J. Kim, R. V Gorbachev, T. Georgiou, S. V Morozov, A. N. Grigorenko, A. K. Geim, C. Casiraghi, A. H. Castro Neto and K. S. Novoselov, *Science (80-.).*, 2013, **340**, 1311–1314.

31 W. J. Yu, Y. Liu, H. Zhou, A. Yin, Z. Li, Y. Huang and X. Duan, *Nat. Nanotechnol.*, 2013, **8**, 952–958.

32 K. W. Seo, J. H. Lee, N. G. Cho, S. J. Kang, H. K. Kim, S. I. Na, H. W. Koo and T. W. Kim, *J. Vac. Sci. Technol. A*, 2014, **32**, 61201.

33 A. Scidà, S. Haque, E. Treossi, A. Robinson, S. Smerzi, S. Ravesi, S. Borini and V. Palermo, *Mater. Today*, 2018, **21**, 223–230.

34 M.-J. Park and J.-S. Lee, *Adv. Electron. Mater.*, 2019, **5**, 1800411.

35 S. Ulstrup, J. C. Johannsen, F. Cilento, J. A. Miwa, A. Crepaldi, M. Zacchigna, C. Cacho, R. Chapman, E. Springate, S. Mammadov, F. Fromm, C. Raidel, T. Seyller, F. Parmigiani, M. Grioni, P. D. C. King and P. Hofmann, *Phys. Rev. Lett.*, 2014, **112**, 257401–257405.

36 J. A. del Alamo, *Nature*, 2011, **479**, 317–323.

37 K. Kim, J.-Y. Choi, T. Kim, S.-H. Cho and H.-J. Chung, *Nature*, 2011, **479**, 338–344.

38 E. Dimakis, J. Lähnemann, U. Jahn, S. Breuer, M. Hilse, L. Geelhaar and H. Riechert., *Cryst. growth Des.*, 2011, **11**, 4001–4008.

39 E. A. Anyebe, Q. Zhuang, A. Sanchez, S. Lawson, A. J. Robson, L. Ponomarenko, A. Zhukov and O. Kolosov., *Rapid Res. Lett.*, 2014, **8**, 658–662.

40 Y. Jing, X. Bao, W. Wei, C. Li, K. Sun, D. P. R. Aplin, Y. Ding, Z.-L. Wang, Y. Bando and D. Wang, *J. Phys. Chem. C*, 2014, **118**, 1696–1705.

41 E. A. Anyebe, Q. Zhuang, B. J. Robinson, O. Kolosov, M. K. Rajpalke, T. D. Veal and V. Falko., *Nano. Lett.*, 2015, **15**, 4348–4355.

42 A. Arlauskas, J. Treu, K. Saller, I. Beleckaitė, G. Koblmüller and A. Krotkus, *Nano Lett.*,

2014, **14**, 1508–1514.

43 K. S. Leschkies, A. G. Jacobs, D. J. Norris and E. S. Aydil, *Appl. Phys. Lett.*, 2009, **95**.

44 A. C. Ford, J. C. Ho, Y.-L. Chueh, Y.-C. Tseng, Z. Fan, J. Guo, J. Bokor and A. Javey, *Nano Lett.*, 2009, **9**, 360–365.

45 M. Abul Khayer and R. K. Lake, *J. Appl. Phys.*, 2010, **107**.

46 Y. Kim, H. J. Joyce, O. Gao, H. H. Tan, C. Jagadish, M. Paladugu, J. Zou and A. A. Suvorova, *Nano Lett.*, 2006, **6**, 599–604.

47 Y. J. Hong, W. H. Lee, Y. Wu, R. S. Ruoff and T. Fukui., *Nano. Lett.*, 2012, **12**, 1431–1436.

48 Y. J. Hong and T. Fukui., *Nano. Lett.*, 2011, **5**, 7576–7584.

49 A. M. Munshi, D. L. Dheeraj, V. T. Fauske, D. C. Kim, A. T. J. van Helvoort, B. O. Fimland and H. Weman, *Nano Lett.*, 2012, **12**, 4570–4576.

50 C. D. Bessire, M. T. Björk, H. Schmid, A. Schenk, K. B. Reuter and H. Riel, *Nano Lett.*, 2011, **11**, 4195–4199.

51 M. Borg, H. Schmid, K. E. Moselund, G. Signorello, L. Gignac, J. Bruley, C. Breslin, P. Das Kanungo, P. Werner and H. Riel, *Nano Lett.*, 2014, **14**, 1914–1920.

52 E. I. Givargizov, J. Cryst. Growth 31, 20 (1975).

53 V. G. Dubrovskii and N. V. Sibirev, Phys. Rev. E 70, 031604 (2004).

54 B. Mandl, A. W. Dey, J. Stangl, M. Cantoro, L.-E. Wernersson, G. Bauer, L. Samuelson, K. Deppert, and C. Thelander, J. Cryst. Growth 334, 51 (2011).

55 I. Vlassiouk, S. Smirnov, I. Ivanov, P. F. Fulvio, S. Dai, H. Meyer, M. Chi, D. Hensley, P. Datskos and N. V Lavrik, *Nanotechnology*, 2011, **22**, 275716.

56 P. G. Klemens and D. F. Pedraza., *Carbon N. Y.*, 1994, **32**, 735–741.

57 E. Pop, V. Varshney and A. K. Roy, *MRS Bull.*, 2012, **37**, 1273.

58 R. S. R. S. Chen, A.L. Moore, W. Cai, J.W. Suk, J. An, C. Mishra, C. Amos, C.W. Magnuson, J. Kang, L. Shi, R.S. RuoffS. Chen, A.L. Moore, W. Cai, J.W. Suk, J. An, C. Mishra, C. Amos, C.W. Magnuson, J. Kang, L. Shi, *ACS Nano*, 2010, **5**, 321.

59 A.A. Balandin, *Nat. Mater.*, 2011, **10**, 569.

60 R. S. R. S. Chen, Q. Wu, C. Mishra, J. Kang, H. Zhang, K. Cho, W. Cai, A.A. Balandin, *Nat. Mater.*, 2012, **11**, 203.

61 A. J. H. McGaughey, E. S. Landry, D. P. Sellan and C. H. Amon, *Appl. Phys. Lett.*, 2011, **99**, 131904.

62 M. Kaviany, *Heat Transfer Physics*, Cambridge University Press, New York, 2008.

63 A. Lizak, and K. Fitzner, *J. Phase Equilibria*, 1994, **15**, 151–154.

64 F. Glas, Ramdani, M. R. Patriarche, G. and J. C. Harmand, Phy. Rev. B. 2013, **88**, 195304.

65 I. Ansara, C. Chatillon, H. L. Lukas, T. Nishizawa, H. Ohtani, K. Ishida, M. Hillert, B. Sundman, B. B. Argent, A. Watson, T. G. Chart, and T. Anderson, Calphad 1994, **18**, 177.